

# MAGNETOSPHERIC ELECTRODYNAMICS: ENERGETIC PARTICLE SIGNATURES OF GEOMAGNETIC STORMS AND SUBSTORMS

Tuija I Pulkkinen

Finnish Meteorological Institute, POBox 503, FIN-00101 Helsinki, Finland

## ABSTRACT

This paper reviews the present understanding of the dynamics of two key magnetospheric disturbances, geomagnetic substorms and storms. Substorms, being the basic dynamic response of the magnetosphere to the varying solar wind conditions, are an important factor in our understanding of the solar wind – magnetosphere coupling processes. On the other hand, the geomagnetic storms represent times when the magnetosphere is under extremely disturbed conditions and are hence of key importance for space weather. The present and future capabilities to forecast when, where, and how intense events occur based on solar or upstream solar wind observations are briefly addressed.

Key words: Magnetosphere, storms, substorms, energetic particles, coronal mass ejections.

## 1. INTRODUCTION

The key issues for space weather can be set in the form of two questions: (1) Event or no event; and (2) If an event does take place, when does it occur, where does it occur, and how intense is it. While the first question can be largely addressed by solar and/or solar wind monitoring, our capability to answer the second question depends critically on our understanding of the physical processes behind the dynamic changes in the near-Earth space.

The magnetosphere is the region of near-Earth space, where the dynamics is governed by the internal geomagnetic field (see Figure 1). The solar wind flow past the Earth distorts the dipole field to compress it on the dayside and elongate it to a long geomagnetic tail on the nightside. The geomagnetic tail plays a key role in magnetospheric dynamics; for example, it acts as an energy reservoir for the dynamic processes.

The magnetosphere comprises distinct regions, which all have their characteristic plasma properties: The tail lobes at high latitudes are regions of low plasma density and energy, whereas the plasma sheet is characterized by denser and hotter  $\sim$ keV plasma. The most hazardous region for technological systems is the inner magnetosphere, where trapped populations of high-energy (from hundreds of keV to multi-MeV)

electrons and ions reside in the ring current and in the van Allen radiation belts.

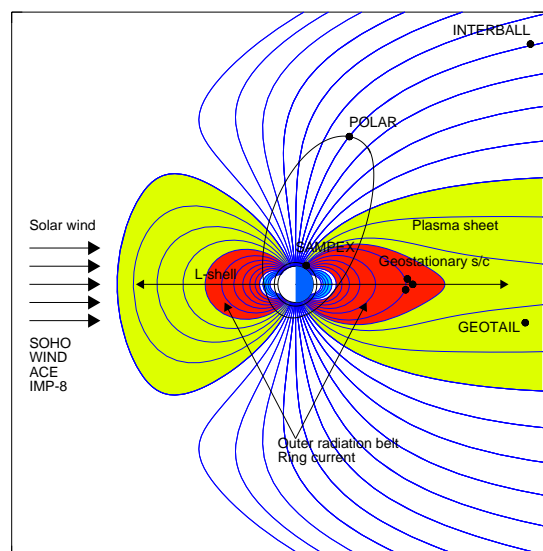


Figure 1. Schematic of the near-Earth magnetosphere. The tail lobes, the plasma sheet (light shading) and ring current/radiation belts (darker shading) are shown. Typical locations of several of the ISTP satellites are also indicated.

The ongoing International Solar Terrestrial Physics (ISTP) program provides an unprecedented opportunity to monitor the near-Earth environment (Acuña et al. 1995). Several spacecraft such as SOHO, WIND, IMP-8, and ACE monitor the Sun and the solar wind almost continuously. Simultaneously, several spacecraft such as POLAR, INTERBALL, and GEOTAIL measure dynamic variations within the magnetosphere. Furthermore, several operational satellites at geostationary orbit or at low-altitude polar orbit together with a multitude of ground-based facilities provide key information of the magnetospheric and ionospheric variability. Hence, the upcoming solar maximum will be monitored with an impressive set of observational facilities that serve as well scientific as operational space weather purposes.

The dynamic response of the magnetosphere to varying solar wind and interplanetary magnetic field conditions is the magnetospheric substorm (Rostoker et al. 1980). Energy input from the solar wind is largely controlled by the interplanetary magnetic field orientation: During periods of southward interplanetary field, the energy input is enhanced and the energy extracted from the solar wind is stored in the magnetosphere in the form of magnetic field energy in the magnetotail. This is the substorm growth phase. After typically 30–60 min, the magnetotail undergoes a change of state from stable to unstable, and the stored energy is dissipated via a highly dynamic process. This substorm expansion phase involves an injection of energetic (tens to hundreds of keV) electrons and ions to the vicinity of the geostationary orbit, strong electric currents in the auroral regions, and rapid fluctuations and configurational changes of the magnetospheric magnetic field. All these phenomena are potential space weather effects. The substorm process ends when the energy dissipation ceases and the magnetosphere recovers its initial state after about two to four hours from the beginning of the event (see Figure 2; for recent reviews see McPherron (1991) and Baker et al. (1996a)).

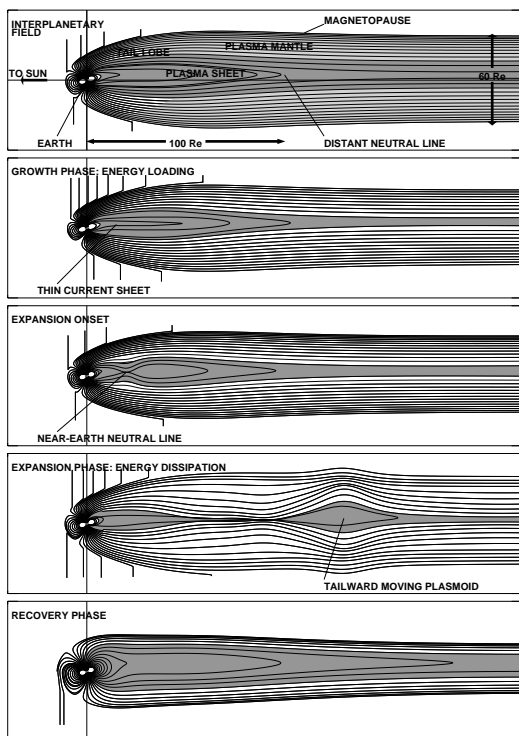


Figure 2. Schematic of the substorm sequence. The figure shows the growth phase-associated thin current sheet formation, plasmoid ejection, and recovery of the initial state. The top panel indicates scale sizes of the system (distance to the Moon is about  $60 R_E$ ).

Geomagnetic storms are large disturbances in the near-Earth environment caused by coherent solar wind and interplanetary field structures that originate from solar disturbances such as coronal mass ejections (Gonzalez et al. 1994). Storms are associated with major disturbances in the in the geomag-

netic field and strong enhancement of the fluxes of energetic (tens to hundreds of keV) ions (??) and high-energy (up to several MeV) electrons in the outer van Allen radiation belt (Baker et al. 1998a). Such activity is clearly a key factor in the problems experienced by space-borne technological systems during disturbed periods (Baker et al. 1996b).

This paper reviews present understanding of the dynamics of the geomagnetic substorms and storms by presenting observations and interpretations of two events, a substorm on Dec 10, 1996 and a storm on May 15, 1997. Both events have been analyzed in detail elsewhere (see Pulkkinen et al. (1998a) and Pulkkinen et al. (1998c) for the substorm event and Baker et al. (1998b) for the storm event), and only a short summary is presented here. Finally, the present and future capabilities to address question (2) are discussed.

## 2. GEOMAGNETIC SUBSTORMS: Dec 10, 1996

The substorm activity on Dec 10, 1996, 06–10 UT, was driven by a period of southward interplanetary magnetic field (IMF). The magnetic field measurements from WIND showed a southward turning at about 0637 UT (see Figure 3). The top panel in Figure 3 show the interplanetary magnetic field (IMF)  $B_Z$  component. The following panels show the  $\epsilon = 10^7 v B^2 l_0^2 \sin^4(\theta/2)$  parameter (in SI units) (Perreault & Akasofu 1978) and its time integral  $\int \epsilon dt$ . The  $\epsilon$  parameter is a measure of the energy input from the solar wind into the magnetosphere; a clear increase is visible after the IMF southward turning. In the plot, the  $\epsilon$  parameter has been time-shifted 7 min to account for the travel time from the s/c location to the subsolar magnetopause.

The following panel shows the AL index as deduced from the CANOPUS ground magnetometer data. The electrojet indices are created from disturbances in the North-South component of auroral-zone magnetograms, and give a measure of the intensity of the ionospheric currents in the auroral zone. The AL index is often used as a measure of substorm intensity. Various studies have shown that the AL index is correlated with the interplanetary magnetic field with an enhancement at about 20-min delay from the IMF southward turning and a larger intensification after about 1 hour of southward IMF (or enhanced energy input (Bargatze et al. 1985)). The start of the substorm growth phase (at 0644 UT) and the substorm onset at 0731 UT are shown with dotted lines in the figure. The global auroral images (data not shown) reveal the large-scale nature of the substorm processes: within only a few tens of minutes, a large portion of the auroral ionosphere – and a large portion of the inner and mid-magnetotail – were influenced by the energy dissipation processes.

The magnetic field at geostationary orbit showed typical growth phase variations, decrease of the northward component shortly after the IMF southward turning. Figure 4 shows the  $H$  component of the magnetic field, which points northward along the dipole axis. GOES 9 at about 2300 MLT was initially outside the disturbance region, and hence observed a further decrease of  $H$  from 0735 to 0740 UT, after

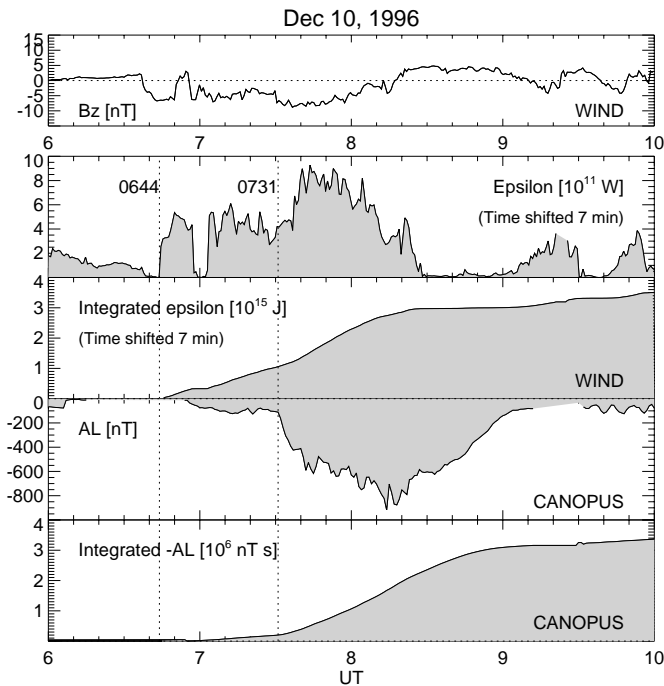


Figure 3. Substorm driver and its effects in the ionosphere. Interplanetary magnetic field  $B_z$  from WIND MFI instrument. The  $\epsilon$  parameter and  $\int \epsilon dt$  computed using the solar wind velocity and magnetic field from WIND. AL index from CANOPUS and its time integral  $\int AL dt$ . (From Pulkkinen et al. 1998b).

which the field gradually became more dipolar; a final, stronger dipolarization occurred after 0810 UT. GOES 8 in the postmidnight sector was to the east of the initial activity region and showed only one gradual dipolarization when the current wedge expanded over the satellite longitude from 0842 UT onward. At 1500 MLT at geostationary orbit, the Los Alamos National Laboratory energetic particle instrument detected enhancements in both proton (50–670 keV) and electron (50–315 keV) fluxes. These enhancements appeared later than the actual substorm activity, as the satellite was far from the substorm onset region.

The signatures introduced here, enhanced energy input caused by southward IMF; enhancement of auroral luminosity and electrojets; stretching of the magnetic field followed by a dipolarization; and enhancement of energetic (tens to hundreds of keV) electrons and protons near geostationary orbit are all typical signatures of the substorm evolution, and their temporal sequence is well-established. The aspect that makes substorms difficult in terms of forecasting is that the relationship between the energy input, storage, and dissipation is highly nonlinear and hence very sensitive to the initial conditions (see e.g. Baker et al. (1996a)). Several attempts to predict e.g. the AL index from upstream data have been made both using nonlinear prediction filters and neural networks (Gleisner & Lundstedt 1997, Klimas et al. 1998a), but the prediction accuracy both in terms of intensity and timing still require refinements in the models.

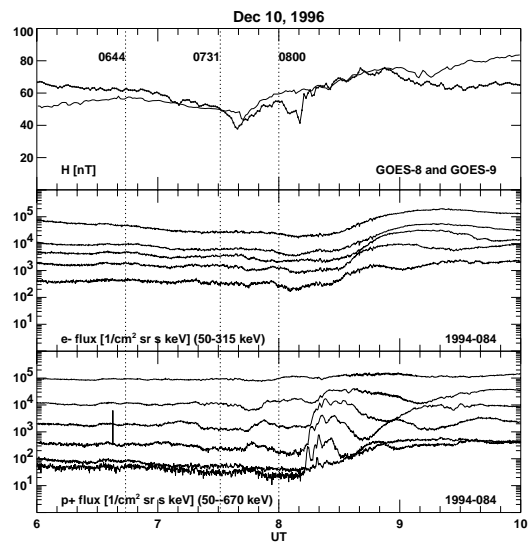


Figure 4. Inner magnetosphere effects of substorm activity. Magnetic field  $H$  component from GOES-9 and GOES-8 spacecraft. Energetic electron (energy range 50–315 keV) and proton (energy range 50–670 keV) measurements from s/c 1994-084. GOES data courtesy of H. Singer; LANL data courtesy of G. Reeves.

### 3. GEOMAGNETIC STORMS: May 15, 1997

An earthward directed, large coronal mass ejection (CME) was observed on May 12, 1997 by the SOHO Extreme ultraviolet Imaging Telescope (EIT) at about 0450 UT (data not shown, see Thompson et al. 1998). The CME created a disturbance (Moreton wave), which in the 195 Å difference images was seen to propagate over the entire visible solar disk. A few hours later, the CME was observed by the Large Angle Spectrometric Coronagraph (LASCO) as a halo event; a bright expanding ring centered around the occulting disk (Brueckner et al. 1998).

The coronal mass ejection expanded from the Sun and was later observed by the WIND spacecraft upstream of the Earth as a magnetic cloud (Baker et al. 1998b). Figure 5 shows the WIND measurements of the total magnetic field, the  $B_z$  component of the field, solar wind velocity and density, and the  $\epsilon$  parameter and its time integral. Note how the strongly southward IMF causes an almost order of magnitude larger peak energy input ( $\epsilon$  value) during the cloud interval. Furthermore, the integrated energy input ( $\int \epsilon dt$ ) during the cloud was a factor of five larger than that associated with the large substorm described in the previous section.

As the cloud reached the Earth, the magnetosphere responded with an increase of the level of activity as recorded by several parameters. The auroral zone magnetograms (CU/CL indices denoting the local AU/AL indices from the Canadian local time sector) showed strong auroral activity reaching 1500 nT, and the geostationary orbit data show large disturbance

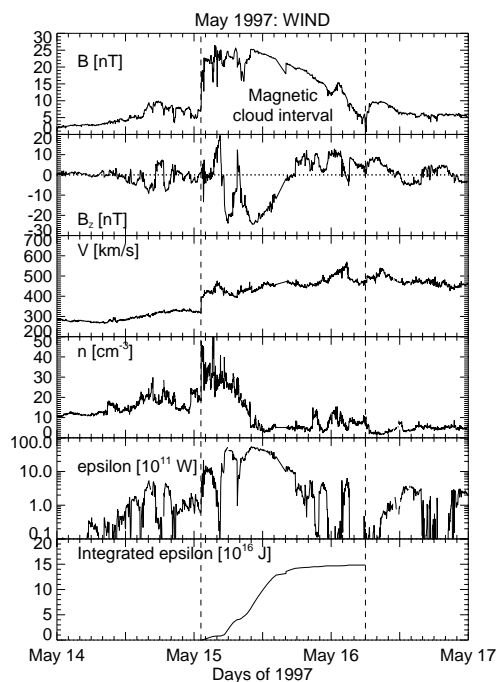


Figure 5. Magnetic cloud in the interplanetary medium. WIND measurements of the total magnetic field,  $B_z$ , solar wind velocity, density,  $\epsilon$  and  $\int \epsilon dt$  computed from the solar wind and IMF parameters. (From Baker et al. 1998b).

levels with several substorm injection events. After the cloud arrival, during the storm main phase, the electron fluxes were extremely variable, reflecting the strong disturbance level of the entire inner magnetosphere (Figure 6).

The Dst-index reached a minimum of  $-169$  nT (Baker et al. 1998b). The Dst index is a measure of the intensity of the ring current carried by energetic ions in the inner magnetosphere ( $L \sim 4 - 7$ ). During the storm main phase the ring current intensifies continuously and hence Dst decreases; the slow recovery that takes from one to several days is associated with the life time of the ring current ions. The Dst index is commonly used as a measure of the geomagnetic storm intensity. Both neural network and nonlinear prediction filter studies relating solar wind parameters and Dst have shown that using L1 measurements and previous values, Dst can be predicted one hour ahead with quite good level of accuracy (Wu & Lundstedt 1997, Klimas et al. 1998b).

The magnetic field at geostationary orbit showed strong fluctuations during the entire period of southward IMF. Furthermore, detailed analysis of the auroral zone ground magnetograms reveals that there was strong ULF wave activity in the frequency range of 2–20 mHz (data not shown; see Baker et al. (1998b)). Near the peak of the storm main phase, a rapid increase in the relativistic electron fluxes was observed at the GOES-8 spacecraft. The rapid in-

crease in the relativistic electron fluxes was associated with the strong substorm activity and the persistent wave activity present in the inner magnetosphere (Baker et al. 1998b). The electron fluxes increased by almost two orders of magnitude, and persisted at the elevated level for several days.

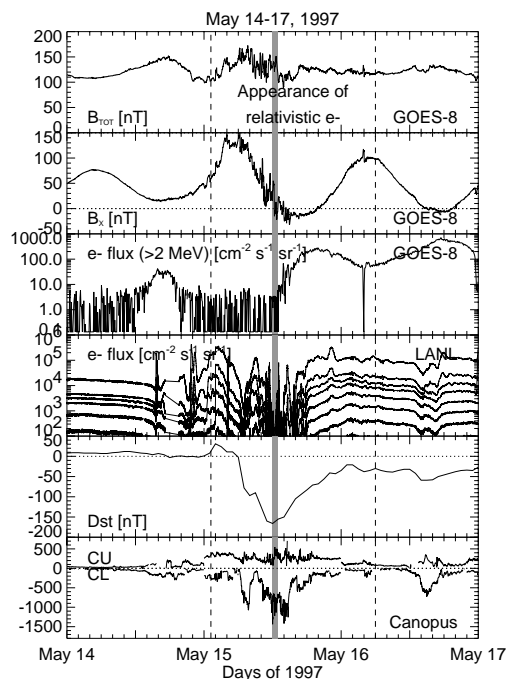


Figure 6. Effects of the magnetic cloud in the magnetosphere and ionosphere. Total magnetic field and  $B_x$  as measured by GOES-8, relativistic electron flux from GOES-8, energetic electron flux from Los Alamos instruments, and ground-based Dst and CU/CL indices. (From Baker et al. 1998b).

Measurements from SAMPEX on a polar orbit at 800 km altitude provide another way to examine the relativistic electron response to the storm activity. Figure 7 shows an L vs time plot of 2–6 MeV electron fluxes throughout the year of 1997. Several intensifications of the electron fluxes are clearly visible, maybe the most notable being the one at the beginning of the year related to the geomagnetic storm on Jan 10, 1997 (Baker et al. 1998a, Reeves et al. 1998). The intensification on May 15, 1997 is distinguished by the large intensity enhancement as well as its low L-shell; flux enhancements extended down to the slot region at  $L < 3$  between the inner and outer radiation belts.

## 4. DISCUSSION

### 4.1. Observational Needs

The key element in all space weather prediction and forecasting activities is continuous monitoring of the

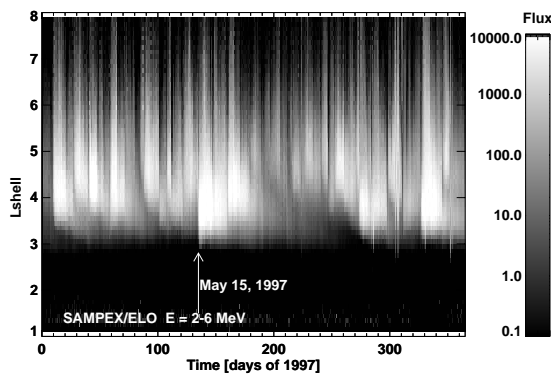


Figure 7. Effects of the magnetic cloud:  $L$ -sorted electron fluxes measured at low altitudes by SAMPEX/ELO for 2–6 MeV. The horizontal axis shows the day of year, the vertical axis shows the magnetic  $L$ -shell, and the electron flux is grey-scale coded according to the scale on the right. Data courtesy of B. Klecker.

Sun and the upstream solar wind. Presently NASA operates two scientific spacecraft (WIND and ACE), which provide almost continuous coverage of solar wind parameters and the interplanetary magnetic field at or close to the L1-point. Measurements made at L1 give about 1 hour warning time under typical solar wind speeds, and provide a reasonably accurate estimate of the plasma and field properties in the vicinity of the Earth. However, differences in the solar wind and IMF front orientations can produce substantial differences in the travel times from L1 to Earth, and if the spacecraft is away from the Sun-Earth line, smaller disturbances may not reach the magnetosphere (Ridley et al. 1998). Hence, two or more spacecraft in the upstream solar wind at different distances would be very advantageous for the forecasting.

It is also important to notice that both ACE and WIND are scientific satellites, which do not have immediate backups if failures would occur. Therefore, a key issue for space weather forecasting in the future is that one or more of the large space agencies would take responsibility for providing continuous series of simple solar wind monitors and their uninterrupted tracking.

At present, SOHO provides an excellent means to monitor the solar activity in great detail. The aim of the ISTP program is to gain better understanding of the Sun-Earth connection, of the chain of events from the surface of the Sun through the magnetosphere, ionosphere, and upper atmosphere. The next few years during the solar maximum will most probably bring major steps forward in our capability to relate the Solar and magnetospheric processes with each other. While unambiguous association of solar and magnetospheric disturbances is more difficult under active conditions, such work is of key importance for space weather predictions (Brueckner et al. 1998, Bothmer & Schwenn 1995).

However, after SOHO the space weather community

needs to consider which solar observations are most critical for the forecasting purposes and what kind of monitors are required in the future. Efforts should already now be focussed to problems of how to predict activity from much less detailed data, and what the minimum requirements for solar observations would be.

## 4.2. Methods for Predicting Substorms and Storms

### 4.2.1. Solar Observations

The best indicators that a coronal mass ejection is on its way toward the Earth are a brightening in the EIT images on the solar disk followed by a halo event in the coronagraph (LASCO) observations. However, Brueckner et al. (1998) studied the correlation of CMEs and geomagnetic activity, and concluded that also other kinds of CMEs than the halo events needed to be included to explain all storms that occurred during the period of investigation. They also concluded that usually it took about 80 hours for the CME to reach the Earth, with a few exceptions with longer delays. Such expansion speeds are consistent with a flux rope model of CME expansion (Chen et al. 1997, Chen 1996). These models provide a good basis for modeling the CME propagation from the Sun to the Earth in order to predict storm occurrence based on solar observations.

### 4.2.2. Physical Models

The global MHD simulations provide at present the only means to physically model the effects of solar wind and IMF variations on the large-scale magnetosphere – ionosphere system. These models accept the solar wind and IMF parameters as input, and then compute the time evolution of the coupled solar wind – magnetosphere – ionosphere system using MHD-equations (Janhunen et al. 1996). At present, there are about ten such simulation codes in the world, one of which in Europe (Bourdarie 1998). The model development and computer resources are at the stage where the results are accurate enough to be compared with actual measurements (Pulkkinen et al. 1998b) and the computations are fast enough to be run in real time. It is to be expected that these models will advance substantially toward operational use during the next few years. Such models can be used equally well for the large disturbances during geomagnetic storms as well as the smaller substorm events.

However, a key factor for space weather is the energetic particle environment in the inner magnetosphere. For MHD simulations, this poses two important problems: First, the models are valid only to  $3.5 R_E$  from the Earth, and hence some boundary effects can occur in the inner magnetosphere. Furthermore, the MHD theory describes the entire plasma with a single temperature, and hence does not provide a means to examine the high-energy particle dynamics. This environment has to be examined using specific models for the radiation belts, which can use the MHD magnetic and electric fields as model input (Bourdarie 1997).

### 4.2.3. Data-derived Models

The nonlinear nature of the solar wind – magnetosphere coupling makes predicting substorm activity difficult. Several authors have studied this coupling using prediction filters and neural network techniques to deduce the geomagnetic indices based only on upstream solar wind measurements and previous time history of the index. These methods have given promising results both on AL index (substorm timing and intensity, Klimas et al. 1998a, Gleisner & Lundstedt 1997) and Dst (storm timing and intensity, Klimas et al. 1998b, Wu & Lundstedt 1997) predictions. Usually, the indices are calculated one hour in advance, and the predictions use the measured values from the previous hour, the solar wind and IMF data as input.

### 4.3. Differences Between Storms and Substorms

Because there are significant differences between the storm and substorm dynamics, the prediction of storms and substorms are quite different problems.

Geomagnetic storms are driven by fast solar wind and/or strong and southward interplanetary magnetic field. Such solar wind/IMF conditions are a consequence of an active event on the Sun. The magnetospheric disturbances are directly driven by the solar wind conditions and last for 1–2 days. Storm-time disturbances accelerate electrons often to MeV energies.

Substorms are smaller disturbances that last 2–4 hours and are driven by southward periods of the interplanetary magnetic field. Such variations are always present in the solar wind; hence substorms occur at a rate of several per day regardless of the solar activity (although substorms are more numerous and stronger during solar maximum than during solar minimum (Nevanlinna & Pulkkinen 1998)). While storms are directly driven by the solar wind and IMF, substorms include also an energy unloading process governed by internal magnetospheric processes. During substorms, particles (both electrons and protons) are typically accelerated to few hundred keV energies. During storms, the particles accelerated by substorms form the seed population that is then further accelerated to the MeV energies (Baker et al. 1998a).

### 4.4. Solar Minimum and Solar Maximum

The Sun is vastly more active during solar maximum than it is during solar minimum, but geomagnetic storms and especially substorms occur also during minimum periods. Notice that both of the events presented in this paper are from the minimum period. Therefore, as technology is and continues to be susceptible to problems caused by the plasma environment, space weather as an issue will not disappear with the next solar maximum. The space physics community is focusing great efforts to monitor, model, and develop theories for the active events that occur during the upcoming solar maximum. The space weather applications will certainly benefit greatly both from the monitoring capabilities

and from the enhanced understanding of the underlying physical processes.

## ACKNOWLEDGMENTS

The author would like to thank K. Ogilvie and R. Lepping for the use of WIND data in this paper, the Canadian Space Agency and the CANOPUS team for the use of CANOPUS magnetometer data, G. Reeves for the LANL energetic particle measurements, H. Singer for the GOES magnetic field and electron data, and B. Klecker for the SAMPEX data.

## REFERENCES

- Acuña, M. H., K. W. Ogilvie, D. N. Baker, S. A. Curtis, D. H. Fairfield, and W. H. Mish, The global geospace science program and its investigations, in *The Global Geospace Mission*, edited by C. T. Russell, p. 5, Kluwer Acad., Dordrecht, the Netherlands, 1995.
- Baker, D. N., T. I. Pulkkinen, V. Angelopoulos, W. Baumjohann, and R. L. McPherron, The neutral line model of substorms: Past results and present view, *J. Geophys. Res.*, *101*, 12,975, 1996a.
- Baker, D. N., J. H. Allen, R. D. Belian, J. B. Blake, S. G. Kanekal, B. Klecker, R. P. Lepping, X. Li, R. A. Mewaldt, K. Ogilvie, T. Onsager, G. D. Reeves, G. Rostoker, H. J. Singer, H. E. Spence, and N. Turner, An assessment of space environmental conditions during the recent Anik E1 spacecraft operational failure, *ISTP Newsletter*, *6*, No 2, June, 1996b (<http://www-istp.gsfc.nasa.gov/istp/newsletter.html>).
- Baker, D. N., T. I. Pulkkinen, X. Li, S. G. Kanekal, J. B. Blake, R. S. Selesnick, M. G. Henderson, G. D. Reeves, and H. E. Spence, Coronal mass ejections, magnetic clouds, and relativistic magnetospheric electron events: ISTP, *J. Geophys. Res.*, *103*, 17279-17292, 1998a.
- Baker, D. N., T. I. Pulkkinen, X. Li, S. G. Kanekal, K. W. Ogilvie, R. P. Lepping, J. B. Blake, L. B. Callis, G. Rostoker, H. J. Singer, and G. D. Reeves, A strong CME-related magnetic cloud interaction with the Earth's magnetosphere: ISTP observations of rapid relativistic electron acceleration on May 15, 1997, *Geophys. Res. Lett.* *25*, 2975, 1998b.
- Bargatze, L. F., D. N. Baker, R. L. McPherron, and E. W. Hones, Jr., Magnetospheric impulse response for many levels of geomagnetic activity, *J. Geophys. Res.*, *90*, 6387, 1985.
- Brueckner, G. E., J.-P. Delaboudiniere, R. A. Howard, S. E. Paswaters, O. C. St. Cyr, R. Schwenn, P. Lamy, G. M. Simnett, B. Thompson, and D. Wang, Geomagnetic storms caused by coronal mass ejections (CMEs): March 1996 through June 1997, *Geophys. Res. Lett.*, *25*, 3019, 1998.
- Bothmer, V., and R. Schwenn, The interplanetary and solar causes of major geomagnetic storms, *J. Geomag. Geoelectr.*, *47*, 1127, 1995.
- Bourdarie, S., D. Boscher, T. Beutier, J.-A. Sauvaud, and M. Blanc, Electron and proton radiation belt

- dynamic simulations during storm periods: a new asymmetric convection–diffusion model, *J. Geophys. Res.*, *102*, 17541, 1997.
- Bourdarie, S., Physical magnetospheric and radiation belt models (MHD and diffusion codes), *this issue*.
- Chen, J., Theory of prominence eruption and propagation: interplanetary consequences, *J. Geophys. Res.*, *101*, 27499, 1996.
- Chen, J., R. A. Howard, G. E. Brueckner, R. Santoro, J. Krall, S. E. Paswaters, O. C. St.Cyr, R. Schwenn, P. Lamy, and G. M. Simnett, Evidence of an erupting magnetic flux rope: LASCO coronal mass ejection of 1997 April 13, *Ap. J.*, *490*, L191, 1997.
- Gleisner, H., and H. Lundstedt, Response of the auroral electrojets to the solar wind modeled with neural networks, *J. Geophys. Res.*, *102*, 14269, 1997.
- Gonzalez, W. D., J. A. Joselyn, Y. Kamide, H. W. Kroehl, G. Rostoker, B. T. Tsurutani, and V. M. Vasyliunas, What is a geomagnetic storm?, *J. Geophys. Res.*, *99*, 5771, 1994.
- Janhunen, P., H. E. J. Koskinen, and T. I. Pulkkinen, A new global ionosphere-magnetosphere coupling simulation utilizing locally varying time step, in: *Third International Conference on Substorms (ICS-3)*, ESA-SP 389, p. 205, 1996.
- Klimas, A. J., J. A. Valdavia, D. Vassiliadis, and D. N. Baker, AL index prediction using data-derived nonlinear prediction filters, *Phys. Space Plasmas* *15*, 1998a.
- Klimas, A. J., D. Vassiliadis, and D. N. Baker, Dst index prediction using data-derived analogues of the magnetospheric dynamics, *J. Geophys. Res.*, *103*, 20435, 1998b.
- McPherron, R. L., Physical processes producing magnetospheric substorms and magnetic storms, in *Geomagnetism*, vol. 4, p. 593, Academic Press, San Diego, CA, 1991.
- Nevanlinna, H., and T. I. Pulkkinen, Solar cycle correlations of substorm and auroral occurrence frequencies, *Geophys. Res. Lett.*, *25*, 3087, 1998.
- Perreault, P., and S.-I. Akasofu, A study of geomagnetic storms, *Geophys. J. R. Astr. Soc.*, *54*, 547, 1978.
- Pulkkinen, T. I., D. N. Baker, L. L. Cogger, T. Mukai, H. J. Singer, Coupling of inner tail and midtail processes, in: *Substorms-4*, edited by S. Kokubun and Y. Kamide, Terra Scientific Publishing Company, Tokyo, p. 749, 1998a.
- Pulkkinen, T. I., D. N. Baker, M. Wiltberger, C. Goodrich, J. G. Lyon, and R. E. Lopez, Pseudobreakup and substorm onset: Observations and MHD simulations compared, *J. Geophys. Res.*, *103*, 14847, 1998b.
- Pulkkinen, T. I., D. N. Baker, L. L. Cogger, L. A. Frank, J. B. Sigwarth, S. Kokubun, T. Mukai, H. J. Singer, K. Ogilvie, J. Slavin, and L. Zelenyi, Spatial extent and dynamics of a thin current sheet during the substorm growth phase on Dec 10, 1996, *J. Geophys. Res.*, submitted, 1998c.
- Reeves, G. D., R. H. W. Friedel, M. G. Henderson, R. D. Belian, M. M. Meier, D. N. Baker, T. Onsager, and H. J. Singer, The relativistic electron response at geosynchronous orbit during the January 1997 magnetic storm, *J. Geophys. Res.*, *103*, 17559, 1998.
- Ridley, A. J., G. Lu, C. R. Clauer, and V. O. Papitashvili, A statistical study of the ionospheric convection response to changing interplanetary magnetic field conditions using the assimilative mapping of ionospheric electrodynamics technique, *J. Geophys. Res.*, *103*, 4023, 1998.
- Rostoker, G., S.-I. Akasofu, J. Foster, R. A. Greenwald, Y. Kamide, K. Kawasaki, A. T. Y. Lui, R. L. McPherron, and C. T. Russell, Magnetospheric substorms - definitions and signatures, *J. Geophys. Res.*, *85*, 1663, 1980.
- Thompson, B. J., S. P. Plunkett, J. B. Gurman, J. S. Newmark, O. C. St.Cyr, and D. J. Michels, SOHO/EIT observations of an Earth-directed coronal mass ejection on May 12, 1997, *Geophys. Res. Lett.*, *25*, 2465, 1998.
- Wu, J.-G. and H. Lundstedt, Geomagnetic storm predictions from solar wind data with the use of dynamic neural networks, *J. Geophys. Res.*, *102*, 14255, 1997.